

Coherent Coupling of Alkali Atoms by Random Collisions

Or Katz,^{1,2} Or Peleg,² and Ofer Firstenberg^{1,*}

¹*Department of Physics of Complex Systems, Weizmann Institute of Science, Rehovot 76100, Israel*

²*Rafael Ltd, IL-31021 Haifa, Israel*

(Received 23 November 2014; published 9 September 2015)

Random spin-exchange collisions in warm alkali vapor cause rapid decoherence and act to equilibrate the spin state of the atoms in the vapor. In contrast, here we demonstrate experimentally and theoretically a *coherent coupling* of one alkali species to another species, mediated by these random collisions. We show that the minor species (potassium) inherits the magnetic properties of the dominant species (rubidium), including its lifetime (T_1), coherence time (T_2), gyromagnetic ratio, and spin-exchange relaxation-free magnetic-field threshold. We further show that this coupling can be completely controlled by varying the strength of the magnetic field. Finally, we explain these phenomena analytically by mode mixing of the two species via spin-exchange collisions.

DOI: 10.1103/PhysRevLett.115.113003

PACS numbers: 33.35.+r, 07.55.Ge, 32.60.+i, 32.80.Xx

Collisions in a warm alkali vapor relax the quantum spin state of the atoms in the vapor. These collisions usually consist of a few spin-destruction collisions, limiting the lifetime (T_1), and of rapid spin-exchange collisions, limiting coherence times (T_2) [1]. Reduced coherence times affect the performance of many vapor physics applications, such as atomic clocks [2], optical memories [3,4], and high-field magnetometers [5]. However, the spin-exchange (SE) relaxation can be completely eliminated in what is known as the spin-exchange relaxation-free (SERF) regime [6,7], allowing the realization of vapor-based ultrasensitive magnetometers [8,9]. In other regimes, SE collisions can be utilized to incoherently transfer polarization between different atomic states [10,11], as is widely used in the production of hyperpolarized noble gases for medical imaging [12], spin-polarized targets [13], and precision measurements [14,15]. The incoherent transfer of polarization via SE collisions was demonstrated in a hybrid system of two alkali species [16,17], improving magnetometry sensitivity by optically pumping one species at a given optical depth and monitoring the other [18]. Transfer of coherence was demonstrated at high magnetic fields for alkali species with the same gyromagnetic ratio, which are naturally coupled [19], and for species with different gyromagnetic ratios, which requires the use of radio-frequency driving fields [20–22]. However, the coherent effects of SE collision at low magnetic fields (the SERF regime) between different species of alkali atoms have never been identified and studied.

In this Letter, we demonstrate a coherent coupling of two alkali species, potassium (K) and rubidium (Rb), induced by random SE collisions. The strength of the coupling is controlled by the strength of the magnetic field. We show that at small magnetic fields, the coupling is strong and the K atoms inherit the magnetic properties of the Rb, including its gyromagnetic ratio (g) and long coherence time (T_2).

Furthermore, the lifetime (T_1) of the K atoms becomes that of the Rb, and the SERF magnetic-field threshold is shown to improve by an order of magnitude, corresponding to that of Rb. We analytically explain these phenomena by SE-induced hybridization of the quantum state of the two species.

When two alkali species coexist in a vapor cell, each atom collides with atoms of its own species (S) at a rate R_{SE}^{S-S} and with atoms of the other species (S') at a rate $R_{SE}^{S-S'}$. Achieving strong coupling between the species requires that $R_{SE}^{S-S'}$ governs the dynamics of S , exceeding both R_{SE}^{S-S} and the Larmor precession rate ω_S . The rate $R_{SE}^{S-S'} = n_{S'} \sigma_{SE}^{S-S'} \bar{v}_T$ depends on the mean thermal velocity \bar{v}_T , the alkali-alkali SE cross section $\sigma_{SE}^{S-S'}$, and the density $n_{S'}$. For Rb and K, the mutual cross section $\sigma_{SE}^{Rb-K} \approx 2 \times 10^{-14} \text{ cm}^{-2}$ is similar to the self cross sections $\sigma_{SE}^{K-K} = 1.5 \times 10^{-14} \text{ cm}^{-2}$ and $\sigma_{SE}^{Rb-Rb} = 1.9 \times 10^{-14} \text{ cm}^{-2}$ [23]. When the two alkali drops are not mixed, the Rb vapor density n_{Rb} is ten times higher than the K density n_K [24]. That is, the SE rate experienced by the K is predominantly determined by the collisions with Rb, $R_{SE}^{K-Rb} \sim 10R_{SE}^{K-K}$, whereas the Rb is only weakly affected by the presence of the K since $R_{SE}^{Rb-Rb} \sim 10R_{SE}^{Rb-K}$. Thus, at high SE rates, the K dynamics will be significantly affected by the presence of the Rb.

To probe the magnetic coherence of the two species we use a single pump and two probe beams as shown in Fig. 1. We use a spherical cell of radius $0.5''$ with a natural abundance of Rb (72% ^{85}Rb and 28% ^{87}Rb) and K, in two separate drops. The cell is heated using a hot air oven to a temperature of $T = 95^\circ\text{C}$, corresponding to number densities of $n_{Rb} \sim 4 \times 10^{12} \text{ cm}^{-3}$ and $n_K \sim 4 \times 10^{11} \text{ cm}^{-3}$. We reduce the radiation trapping and collision rate with the cell walls by introducing 200 torr of N_2 buffer gas. The magnetic field is controlled by shielding the cell with μ -metal cylinders and three perpendicular Helmholtz coils.

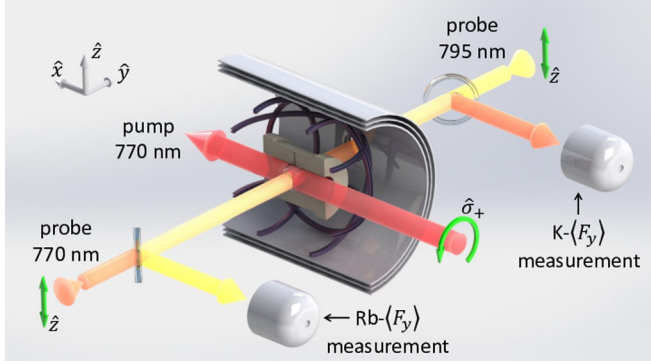


FIG. 1 (color online). Schematics of the experimental setup. The K atoms are initially polarized by a σ_+ -polarized pumping beam. The polarization rotation of two linearly polarized beams (770 nm and 795 nm) is measured to probe the atomic spin precession of both K and Rb atoms, after a magnetic field B_z is applied.

We apply a magnetic field B_x and optically pump the K using a circularly polarized laser beam at 770 nm along the \hat{x} direction. The beam is wider than the cell with intensity of 1 mW/cm^2 , tuned to the $D1$ absorption peak. During the pumping, the K atoms pump the Rb atoms via SE collisions. We then switch off the pumping light and apply a magnetic field $B\hat{z}$. Consequently, both Rb and K spins precess around the magnetic field while decaying due to the various relaxation mechanisms in the cell. We monitor this precession by measuring the optical rotation of linearly polarized probe beams at 770 nm and 795 nm, close to resonance with the K and Rb, respectively. We ensure that the probes do not induce relaxation by using moderate intensities ($I_{\text{Rb}} = 1 \text{ mW/cm}^2$, $I_{\text{K}} = 10 \text{ mW/cm}^2$) and detuning from the $D1$ line [$\Delta\nu_{\text{Rb}} = 25(2\pi) \text{ GHz}$, $\Delta\nu_{\text{K}} = 15(2\pi) \text{ GHz}$]. As a reference, we measured the magnetic coherence of K in a similar cell, without Rb.

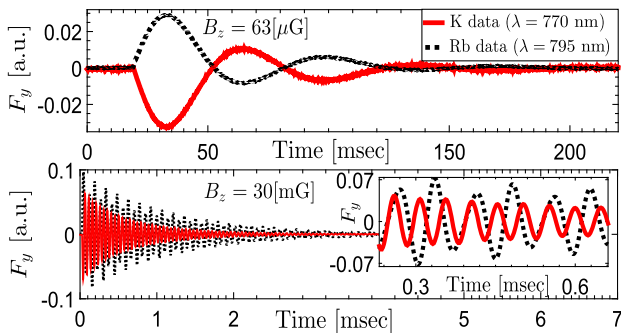


FIG. 2 (color online). Typical measurement of F_y (the \hat{y} component of the spin) for K and Rb. At low magnetic fields (top panel), the two species are coherently coupled (they oscillate and decay at the same rate), while at high magnetic fields (bottom panel), they are decoupled (they oscillate and decay differently). We note that the opposite phase of the signals results from the counterpropagating arrangement of the probing beams.

A typical measurement of the optical rotation signals at low and high magnetic fields is shown in Fig. 2. At high magnetic fields, the two species are weakly coupled and oscillate at different frequencies $\omega_{\text{K}} = 1.5\omega_{\text{Rb}}$, corresponding to their natural gyromagnetic ratios [6],

$$g = \frac{\mu_B g_s}{\hbar} \frac{1}{(2I+1)}, \quad (1)$$

where $I_{\text{ssRb}} = 5/2$, $I_{\text{K}} = 3/2$, and $g_s = 2$. However, at low magnetic fields, the two species are strongly coupled and thus precess at the same frequency and have the same decoherence rate. The frequencies and decoherence rates were determined by fitting each signal to the simple equation $f = \sum_{i=1,2} c_i e^{-\Gamma_i t} \sin(\omega_i t + \varphi_i)$, assuming that c_i , Γ_i , ω_i , and φ_i are constant fit parameters. The beating of the Rb signal (Fig. 2, bottom) originated from the presence of the ^{87}Rb isotope, and its effect on the K dynamics is discussed in the Supplemental Material [25]. At low and high magnetic fields, each signal has a single dominant precession rate ω_i with a corresponding decoherence rate Γ_i . Therefore, in these regimes, we identify for each species the dominant precession rate ω_{K} , ω_{Rb} and the decoherence rate Γ_{K} , Γ_{Rb} (shown in Fig. 3).

The *coherent* coupling is demonstrated in Fig. 3(a) by examining the precession rates of the two species. While the gyromagnetic ratio of the Rb is practically unaffected by the presence of the K (corresponding to its normal SERF behavior [6,7]), the K dynamics is strongly influenced by the Rb. At high magnetic fields, the K is well decoupled and precesses at its natural rate, $g = 0.7(2\pi) \text{ MHz/G}$. However, at low magnetic fields, the coupling is strong and the K precesses at the gyromagnetic ratio of Rb, $g = 0.26(2\pi) \text{ MHz/G}$, and not at its natural low-field precession rate [6,7], $g = 0.46(2\pi) \text{ MHz/G}$.

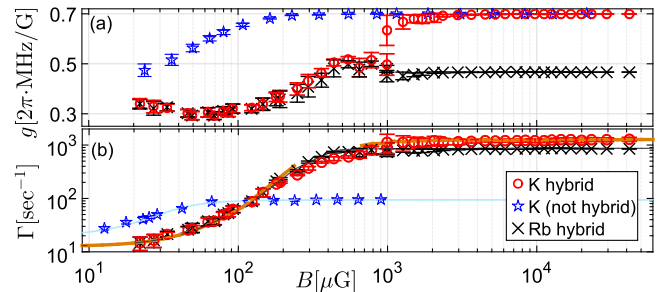


FIG. 3 (color online). (a) Measured gyromagnetic ratios $g = \omega/B_z$ of Rb (black) and K (red) in the hybrid cell. The K inherits the precession rate of Rb at low magnetic fields. The measured g of K in a reference cell without Rb is shown for comparison (blue). (b) Measured decoherence rate $\Gamma = 1/T_2$ of the two species. Γ_{K} is significantly improved at low magnetic fields. Both species experience SERF at the same magnetic-field threshold, ten times higher than the threshold of K without Rb. The solid lines are the analytically calculated values.

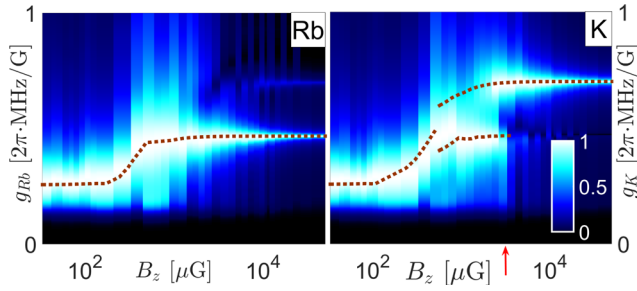


FIG. 4 (color online). Spectral content of the measured signals as a function of the magnetic field. The vertical axis is scaled to measure the gyromagnetic ratio. The Rb precesses at a single rate (left panel) while the K inherits the rate of the Rb at low fields. The theoretical g is plotted with dashed lines.

To investigate the transition between the coupled and uncoupled states of the two species, we show in Fig. 4 the spectral dependence of the signals on the applied magnetic field. We plot the FFT of the measured signals at different magnetic fields using a normalized scale ($\omega \rightarrow \omega/B_z$) corresponding to the gyromagnetic ratio g (for visualization purposes, we replace with zero the FFT around $g = 0$). At high and low magnetic fields, the physics is exactly the same as in Fig. 3(a): the two species share the same gyromagnetic ratio (that of the Rb) at low fields, while reaching their normal different values at high magnetic fields. However, at intermediate fields, the K precesses at a combination of two frequencies, both at its natural precession rate and at the rate of ^{85}Rb (most clearly visible at $B_z = 3$ mG; the red arrow in Fig. 4). The nature of this transition cannot be explained by a mere shift in the slowing-down factor since the K dynamics consists of two distinct frequencies. Thus, the minor species (K) is coherently coupled to the dominant species (Rb) at low magnetic fields by SE collisions, and the coupling strength is controlled by the magnitude of the magnetic field.

This coherent coupling alters significantly other important properties of the K. While the relaxation rate $\Gamma_{\text{Rb}}(B_z)$ is unaffected by collisions with K (SE relaxation is eliminated at $\omega_{\text{Rb}} \lesssim R_{\text{SE}}^{\text{Rb-Rb}}$ [6], as if the K is absent), the relaxation rate $\Gamma_{\text{K}}(B_z)$ is inherited from the Rb, as shown in Fig. 3(b). Consequently, the relaxation rate $\Gamma_{\text{K}}(B_z)$ decreases dramatically at low magnetic fields, in comparison to a cell without Rb. The elimination of relaxation of the K atoms appears at $\omega_{\text{K}} \lesssim R_{\text{SE}}^{\text{Rb-K}}$, i.e., at magnetic fields ten times higher (less stringent) than those required without the Rb, $\omega_{\text{K}} \lesssim R_{\text{SE}}^{\text{K-K}}$. Thus, the dominant species (Rb) drives the minor species (K) into SERF at the magnetic-field threshold of the dominant species. At high magnetic fields, the relaxation of the minor species is increased due to mutual SE collisions. Furthermore, we measure an identical lifetime of both species ($T_1 = 86 \pm 1$ msec). Via collisions, the K inherits the lifetime of the Rb incoherently, as theoretically explained for different isotopes in Ref. [11].

Since the spin destruction is dominated by electron-randomizing collisions (e.g., anisotropic collisions with N_2), the K benefits from the larger nuclear spin reservoir of the Rb. Therefore, through collisional induced coherent coupling, the minor species (K) inherits the magnetic properties of the dominant species (Rb), including its precession rate, decoherence rate, lifetime, and SERF magnetic field threshold.

To understand the nature of the coherent coupling, we solve the coupled Liouville equations describing the dynamics of the system. Because of frequent SE collisions, the coherence between the two hyperfine levels decays rapidly. Therefore, the ground-state density matrix of each species s can be simplified by decomposing ρ^s into a two block diagonal form $\rho^s = \rho_a^s + \rho_b^s$, where $a = I_S + 1/2$ denotes the higher hyperfine level and $b = I_S - 1/2$ the lower one [26]. The Larmor coherence can be described by the transverse spin vector $\langle F_{+}^s \rangle \equiv -F_x^s + iF_y^s = F_{a+}^s + F_{b+}^s$, where we omit the brackets $\langle \rangle$ for brevity. In the absence of the mutual SE interaction, the dynamics of F_{+}^s for each species is given by [25]

$$\frac{d}{dt} \begin{pmatrix} F_{a+}^s \\ F_{b+}^s \end{pmatrix} = \begin{pmatrix} -ig_s B_z & 0 \\ 0 & -1 \end{pmatrix} - R_{\text{SE}}^{s-s} \begin{pmatrix} x_a^s & y^s \\ y^s & x_b^s \end{pmatrix} - R_{\text{SD}}^{s-s} \begin{pmatrix} w_a^s & z^s \\ z^s & w_b^s \end{pmatrix} \begin{pmatrix} F_{a+}^s \\ F_{b+}^s \end{pmatrix}, \quad (2)$$

where g_s is the gyromagnetic ratio of each species [Eq. (1)], R_{SD}^{s-s} is the spin-destruction rate, and the constant coefficients $w_a^s, w_b^s, x_a^s, x_b^s, y^s, z^s$ are given in Ref. [25], depending on the nuclear spin I_S only. The SE coupling between the two species supplements Eq. (2) by inducing the coupling interaction

$$\frac{d}{dt} (\tilde{\mathbf{F}}_{+})_{\text{coupling}} = -\vec{M} \cdot \tilde{\mathbf{F}}_{+}, \quad (3)$$

where $\tilde{\mathbf{F}}_{+}$ denotes the four-component vector $\tilde{\mathbf{F}}_{+} \equiv (F_{a+}^{\text{Rb}}, F_{b+}^{\text{Rb}}, F_{a+}^{\text{K}}, F_{b+}^{\text{K}})$ and \vec{M} is the 4×4 linearized SE coupling matrix, given by

$$\vec{M} = \text{diag} \begin{pmatrix} R_{\text{SE}}^{\text{Rb-K}} \\ R_{\text{SE}}^{\text{Rb-K}} \\ R_{\text{SE}}^{\text{K-Rb}} \\ R_{\text{SE}}^{\text{K-Rb}} \end{pmatrix} \begin{pmatrix} w_a^{\text{Rb}} & z^{\text{Rb}} & G_{11}^{\text{Rb}} & G_{12}^{\text{Rb}} \\ z^{\text{Rb}} & w_b^{\text{Rb}} & G_{21}^{\text{Rb}} & G_{22}^{\text{Rb}} \\ G_{11}^{\text{K}} & G_{21}^{\text{K}} & w_a^{\text{K}} & z^{\text{K}} \\ G_{12}^{\text{K}} & G_{22}^{\text{K}} & z^{\text{K}} & w_b^{\text{K}} \end{pmatrix}. \quad (4)$$

Here, the constants $G_{11}^s, G_{12}^s, G_{21}^s, G_{22}^s$ depend on I_{Rb} and I_{K} only [25]. Qualitatively, this coupling interaction has two major effects on the dynamics of the vapor. First, it increases the effective spin-destruction rate of the two species, by $R_{\text{SE}}^{\text{Rb-K}}$ for the Rb and $R_{\text{SE}}^{\text{K-Rb}}$ for the K, as can be

seen by the block-diagonal elements in Eq. (4). Second, since $R_{SE}^{K-Rb} \gg R_{SE}^{K-K}, R_{SD}^{K-K}$, the coupling through the coefficients G_{ij}^K becomes the dominant collisional interaction for the K, while the coupling experienced by the Rb is weak, since $R_{SE}^{Rb-K} \ll R_{SE}^{Rb-Rb}$. At low magnetic fields, R_{SE}^{K-Rb} is the dominant rate for the K spins, which therefore respond to the precession of the Rb spins as forced oscillations and inherit the Rb magnetic properties. At the same time, the Rb dynamics remain unaffected by the K.

To quantitatively describe this coupling, we solve the two coupled equations (2) and (3) by diagonalizing the 4×4 matrix and calculating the eigenvalues λ_i of the four eigenmodes $|\lambda_i\rangle$. Each spin component of $\tilde{\mathbf{F}}_+^i$ can be spanned by the eigenmodes,

$$\tilde{\mathbf{F}}_+^i(t) = \tilde{\mathbf{F}}_+^i(0) \sum_{j=1}^4 p_{ij} e^{\lambda_j t}, \quad (5)$$

where the coefficients p_{ij} satisfy the normalization condition $\sum_j p_{ij} = 1$. The decoherence rates and gyromagnetic ratios of the eigenmodes, corresponding to $\Gamma_i = -\text{Re}(\lambda_i)$ and $g_i = \text{Im}(\lambda_i/B_z)$, respectively, are shown in Fig. 5 (top panels). At high magnetic fields, the gyromagnetic ratios $g_1 = -g_4 = 0.47(2\pi)$ MHz/G correspond to the precession rate of ^{85}Rb , while $g_2 = -g_3 = 0.7(2\pi)$ MHz/G correspond to the rate of K [Eq. (1)]. The sign of g corresponds to the corotation of the upper hyperfine level (a) for a positive value and counterrotation of the lower level and (b) for a negative value. Γ_1 remains the lowest decay rate of the system at all magnetic fields. As the magnetic field is lowered, $\Gamma_1(B)$ decreases (experiencing SERF), and consequently $|\lambda_1\rangle$ becomes the dominant eigenmode.

To infer the dynamics of the atoms, we plot the coefficients p_{ij} of each species in Fig. 5 (bottom panels). At high magnetic fields, the eigenmodes are well resolved, corresponding to $|\lambda_1\rangle$ for F_{a+}^{Rb} , $|\lambda_2\rangle$ for F_{a+}^K , $|\lambda_3\rangle$ for F_{b+}^K , and $|\lambda_4\rangle$ for F_{b+}^{Rb} . Consequently, the different hyperfine

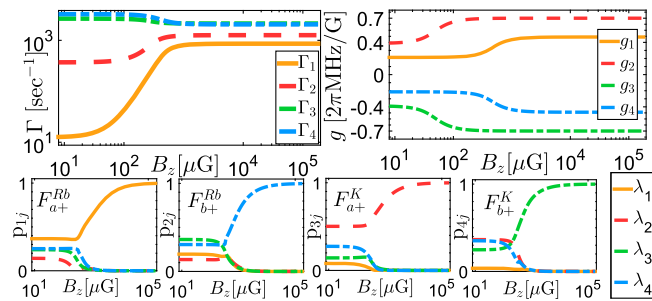


FIG. 5 (color online). Theoretical results. (Top panels) Decoherence rates $-\text{Re}(\lambda)$ (left panel) and gyromagnetic ratios $\text{Im}(\lambda/B_z)$ (right panel) of the four eigenmodes. The decoherence rate Γ_1 vanishes at low magnetic fields due to SERF. (Bottom panels) The coupling coefficients p_{ij} of the four spin components. At high magnetic fields, the spins of K and ^{85}Rb consist of a single mode; at low fields, the spins consist of all modes, and thus share their coherence.

levels remain resolved, such that each magnetic coherence rotates at its natural rate g_i . As the magnetic field is lowered, $\tilde{\mathbf{F}}_+^i$ becomes a mixture of the four different modes, inducing mixing between the different hyperfine levels of both species. Since at low magnetic fields $\Gamma_1 \ll \Gamma_2, \Gamma_3, \Gamma_4$, eigenmode $|\lambda_1\rangle$ dominates; the K and Rb spins precess and decay at the same rate and experience SERF at the Rb's transition rate. This common effectively single eigenmode shows that, at low magnetic fields, the two species hybridize by the SE interaction. At intermediate magnetic fields, Γ_1 increases and more eigenmodes become important, resulting in multiple decoherence and precession rates for each species, especially for the minor one (K). At this transition regime, the high decoherence rates $\Gamma_i \gtrsim \omega_i - \omega_j$ broaden the spectral profile of the signals, as observed in Fig. 4.

To make a comparison with the experiment, the theoretical decoherence rate and gyromagnetic ratio are plotted in Figs. 3 and 4. These parameters were evaluated from Eq. (5), while taking into account the presence of ^{87}Rb in our experiment [25], without any free parameters. Γ_{Rb} is almost unaffected by the presence of K and has a single decoherence rate and gyromagnetic ratio at any magnetic field. The K is governed by a single mode at low and high magnetic fields and by multiple modes at intermediate fields. Therefore, in this region, we do not associate a single Γ_K and show the two dominant frequencies in Fig. 4. Our theoretical model appears to fully describe the physics of the interaction and the hybridization of the species.

The SE hybridization of different alkali species could be used for sensors and quantum-information applications. Such applications require the use of an optically thick medium to achieve a high efficiency and signal-to-noise ratio [27]. If a minor species is added with low optical depth (OD), it can be efficiently pumped into a nondegenerate coherent dark state, and it can transfer this coherent state to a dominant species through the coherent SE coupling. The dominant species can then be optically addressed to benefit from its higher OD. A possible outcome is a new mechanism to interface vapor-based quantum memories, by storing light on one species and extracting it efficiently from another species.

In conclusion, we show in this Letter that random SE collisions coherently couple two different alkali species. The coupling strength is controlled by the magnitude of the magnetic field. At low magnetic fields, a minor species is strongly coupled to the dominant species and, as a result, inherits the magnetic properties of the dominant species, such as the coherence-time and gyromagnetic ratio. At intermediate magnetic fields, we measure a unique response of the minor species, consisting of two precession rates. At high magnetic fields, the two species become decoupled. We explain these phenomena by showing analytically that, by lowering the magnetic field, the minor species starts sharing the main eigenmode of the dominant

species. This effect may be utilized in different magnetometry and quantum-information schemes.

We thank Mark Dikopoltsev and Elad Greenfeld for their valuable help in preparing the cell. This work was supported by the Israel Science Foundation, by Leon and Blacky Broder, and by the Sir Charles Clore research prize.

*Corresponding author.

ofer.firstenberg@weizmann.ac.il

- [1] W. Happer, *Rev. Mod. Phys.* **44**, 169 (1972).
- [2] S. A. Zibrov, I. Novikova, D. F. Phillips, R. L. Walsworth, A. S. Zibrov, V. L. Velichansky, A. V. Taichenachev, and V. I. Yudin, *Phys. Rev. A* **81**, 013833 (2010).
- [3] D. F. Phillips, A. Fleischhauer, A. Mair, R. L. Walsworth, and M. D. Lukin, *Phys. Rev. Lett.* **86**, 783 (2001).
- [4] M. Shuker, O. Firstenberg, R. Pugatch, A. Ron, and N. Davidson, *Phys. Rev. Lett.* **100**, 223601 (2008).
- [5] D. Budker and M. V. Romalis, *Nat. Phys.* **3**, 227 (2007).
- [6] W. Happer and A. C. Tam, *Phys. Rev. A* **16**, 1877 (1977).
- [7] O. Katz, M. Dikopoltsev, O. Peleg, M. Shuker, J. Steinhauer, and N. Katz, *Phys. Rev. Lett.* **110**, 263004 (2013).
- [8] J. C. Allred, R. N. Lyman, T. W. Kornack, and M. V. Romalis, *Phys. Rev. Lett.* **89**, 130801 (2002).
- [9] R. Mhaskar, S. Knappe, and J. Kitching, *Appl. Phys. Lett.* **101**, 241105 (2012).
- [10] T. G. Walker and W. Happer, *Rev. Mod. Phys.* **69**, 629 (1997).
- [11] S. Appelt, A. B. Baranga, C. J. Erickson, M. Romalis, A. R. Young, and W. Happer, *Phys. Rev. A* **58**, 1412 (1998).
- [12] S. B. Fain, F. R. Korosec, J. H. Holmes, R. O'Halloran, R. L. Sorkness, and T. M. Grist, *Magn. Reson. Imaging* **25**, 910 (2007).
- [13] T. Katabuchi, S. Buscemi, J. M. Cesaratto, T. B. Clegg, T. V. Daniels, M. Fassler, R. B. Neufeld, and S. Kadlecsek, *Rev. Sci. Instrum.* **76**, 033503 (2005).
- [14] G. Vasilakis, J. M. Brown, T. W. Kornack, and M. V. Romalis, *Phys. Rev. Lett.* **103**, 261801 (2009).
- [15] M. Smiciklas, J. M. Brown, L. W. Cheuk, S. J. Smullin, and M. V. Romalis, *Phys. Rev. Lett.* **107**, 171604 (2011).
- [16] E. Babcock, I. Nelson, S. Kadlecsek, B. Driehuys, L. W. Anderson, F. W. Hersman, and T. G. Walker, *Phys. Rev. Lett.* **91**, 123003 (2003).
- [17] B. Lancor and T. G. Walker, *Phys. Rev. A* **83**, 065401 (2011).
- [18] M. V. Romalis, *Phys. Rev. Lett.* **105**, 243001 (2010).
- [19] T. Ito, N. Shimomura, and T. Yabuzaki, *J. Phys. Soc. Jpn.* **72**, 1302 (2003).
- [20] S. Haroche and C. Cohen-Tannoudji, *Phys. Rev. Lett.* **24**, 974 (1970).
- [21] H. Ito, T. Ito, and T. Yabuzaki, *J. Phys. Soc. Jpn.* **63**, 1337 (1994).
- [22] T. Ito, N. Shimomura, and T. Yabuzaki, *J. Phys. Soc. Jpn.* **64**, 2848 (1995).
- [23] This is because the collisions involve only the outer electrons of the colliding pair [1].
- [24] D. Lide, *Handbook of Chemistry and Physics*, 85th ed. (CRC, Boca Raton, FL, 2004).
- [25] See Supplemental Material at <http://link.aps.org/supplemental/10.1103/PhysRevLett.115.113003> for a comprehensive description of Bloch equations derivation and the effect of ^{87}Rb on the dynamics of the vapor.
- [26] I. M. Savukov and M. V. Romalis, *Phys. Rev. A* **71**, 023405 (2005).
- [27] M. Lukin, *Rev. Mod. Phys.* **75**, 457 (2003).